ResearchGate

See discussions, stats, and author profiles for this publication at: https://www.researchgate.net/publication/256454067

# Probing disorder and transport properties in polypyrrole thin-film devices by impedance and Raman spectroscopy

**Article** *in* Journal of Physics D Applied Physics · September 2013

DOI: 10.1088/0022-3727/46/36/365306

CITATIONS
53

READS
5,205

**5 authors**, including:

Vaibhav Varade
Indian Institute of Science
**12** PUBLICATIONS **185** CITATIONS
SEE PROFILE

Gajanan V Honnavar
PES University EC Campus
**23** PUBLICATIONS **96** CITATIONS
SEE PROFILE

Anjaneyulu Ponnam
Reva University
**19** PUBLICATIONS **193** CITATIONS
SEE PROFILE

K. P. Ramesh
Indian Institute of Science
**142** PUBLICATIONS **1,414** CITATIONS
SEE PROFILE

**Some of the authors of this publication are also working on these related projects:**



IISc PhD. View project



conducting polymers View project

All content following this page was uploaded by Vaibhav Varade on 08 August 2014.

The user has requested enhancement of the downloaded file.

IOPscience iopscience.iop.org

Home Search Collections Journals About Contact us My IOPscience

Probing disorder and transport properties in polypyrrole thin-film devices by impedance and Raman spectroscopy

This content has been downloaded from IOPscience. Please scroll down to see the full text.

2013 J. Phys. D: Appl. Phys. 46 365306

(http://iopscience.iop.org/0022-3727/46/36/365306)

View the table of contents for this issue, or go to the journal homepage for more

Download details:

IP Address: 203.200.43.195
This content was downloaded on 08/08/2014 at 14:04

Please note that terms and conditions apply.

J. Phys. D: Appl. Phys. **46** (2013) 365306 (8pp) doi:10.1088/0022-3727/46/36/365306

# Probing disorder and transport properties in polypyrrole thin-film devices by impedance and Raman spectroscopy

**Vaibhav Varade[1], Gajanan V Honnavar[1,2], P Anjaneyulu[1], K P Ramesh[1] and Reghu Menon[1]**

[1] Department of Physics, Indian Institute of Science, Bangalore 560012, India
[2] PES Institute of Technology, Bangalore South Campus, Bangalore 560100, India

E-mail: vaibhav.tvarade@gmail.com

Received 4 May 2013, in final form 9 July 2013
Published 22 August 2013
Online at stacks.iop.org/JPhysD/46/365306

**Abstract**
In the present study, impedance and Raman spectroscopy are adopted to probe the nature and extent of disorder to correlate with transport properties in doped polypyrrole (PPy) thin-film devices, synthesized electrochemically at different temperatures. A comparative study of the impedance spectroscopy is performed on PPy devices by both experimental and simulation approach with varying extent of disorder. The impedance measurements of PPy devices are well described by introducing a constant phase element (CPE) ($Q$) in modified $RQ$ circuit, which accounts for frequency dependence of dielectric response. However, for the PPy grown at lower temperature, an equivalent circuit consisting of two such $RQ$ elements in series is used for successful modelling of the impedance results, which accounts for the depletion region near the electrode. Raman spectroscopy and the de-convoluted spectra are successfully studied to probe the variation in C=C bond stretching and distribution of conjugation length, which relates to disorder in PPy films and the interpretation is well correlated to the impedance results.

(Some figures may appear in colour only in the online journal)

## 1. Introduction

Disordered and amorphous materials such as glass and polymers have been a fascinating field of research in recent decades in both commercial and scientific aspects [1]. Conducting polymers (CPs) with an extended $\pi$-electron system are one of the widely studied disordered materials due to their potential advantages such as low cost, easy processing, light weight and flexibility [2]. Polypyrrole (PPy) is one of the most studied CPs since the discovery of CPs [3, 4]. PPy is also one of the most important CPs because of its facile synthesis, good environmental stability and high conductivity, which make it promising for commercial applications. PPy has been found useful in various applications such as gas sensors, biosensors, microactuators, supercapacitors, electrochromic windows, polymeric batteries, solar cells and electronic devices such as field-effect transistors [5–10]. Usually thin films of the PPy are synthesized by electropolymerization and PPy powders (pyrrole black) are obtained by chemical oxidative polymerization [11]. Conductivity values up to 2000 S cm$^{-1}$ have been achieved in the case of PPy by freezing interfacial polymerization method [12]. Both electrical and mechanical properties of the PPy depend upon the extent and type of the structural disorder present in the system. In electropolymerized PPy, disorder can be altered by varying conditions such as temperature and pH values of the electrolyte [11]. Doping and de-doping processes also give rise to disorder in CPs and can tune the Fermi levels of the CPs to achieve suitable conductivities for research and applications [13]. Due to large diversity associated with the synthesis processes of CPs, transport mechanism is still a considerable subject of research in this field. Since disorder plays a key role in inducing and deciding the charge transport properties in CPs, it becomes important to probe the disorder and correlate it with transport phenomena in these complex systems.

Impedance and Raman spectroscopies have been the useful techniques for investigating electrical/dielectric and structural properties of the organic and inorganic

 © 2013 IOP Publishing Ltd Printed in the UK & the USA

semiconductors/devices [14–16]. Under different conditions, impedance spectroscopy can be used to obtain relevant information such as formation of granular boundaries and redox dynamics of CPs in electrochemical processes [17]. With impedance spectroscopy, the data can be modelled in terms of equivalent circuit which gives an insight into transport mechanisms of material and device operation. In recent studies, impedance spectroscopy has been used to analyse charge carrier density, diffusion and recombination in polymer blends with contact electrodes [14]. In addition, impedance measurements can also provide information about disorder in terms of nanoscale connectivity and correlation lengths in the system [18, 19]. Raman spectroscopy has become a useful tool for probing structures, disorder, bond length, lattice distortions/interactions and doping level in the disordered systems [20–23]. For example, the effect of annealing on the morphology in bulk heterojunction polymer devices has been investigated recently by using Raman spectroscopy [21]. Moreover, Raman studies on CPs can also provide useful information regarding the presence of polarons and bi-polarons which contributes to charge transport [24, 25]. On one hand, impedance spectroscopy sheds light on inhomogeneity and disorder in material as well as mechanisms and operations of the charge transport, while on the other hand Raman spectroscopy gives information about structural morphology and bond interactions. A corroborative study using these techniques is lacking in the case of electropolymerized CPs and is essential to correlate transport and structural properties.

In the present study, we have used impedance and Raman spectroscopies to investigate the disorder present in PPy thin films and to understand the dependence of transport properties on the nature and extent of the disorder. Different PPy thin-film samples are synthesized electrochemically with different extent of disorder introduced by varying synthesis temperature. Using modelled equivalent circuits and de-convoluted Raman spectra of the samples, an effort is made to understand and correlate the results obtained by both impedance and Raman spectroscopies.

## 2. Experiment

Distilled pyrrole (Aldrich) and propylene carbonate (Aldrich) were used for solution preparation. Synthesis solution was made of 0.06M pyrrole and $TBAPF_6$ (serves as both electrolyte and dopant) in propylene carbonate. The solution was purged with nitrogen gas for 30 min before starting the film synthesis. Working electrodes were prepared by sputtering 100 nm thick platinum on 20 nm thin chromium layer on a 1 $cm^2$ glass slide, while thin stainless steel foil was used as the counter electrode. Electrodes were cleaned with triple-distilled water, acetone and isopropyl alcohol. The PPy films were synthesized galvanostatically in electrochemical cell under nitrogen atmosphere. Synthesis temperature was maintained using a thermal bath. Four doped PPy films, PPy1, PPy2, PPy3 and PPy4 were synthesized at 30 °C, 0 °C, −10 °C and −20 °C, respectively, by passing ∼4 mA $cm^{-2}$ of current for 1 min. The samples were cleaned with isopropyl alcohol and then vacuum dried for 12 h. The thickness of all the samples was measured using a Dektak surface profilometer and found to be around 1 $\mu$m. Energy dispersive spectroscopy (EDS) is performed on the samples and doping level (a ratio between total percentages of phosphorus and nitrogen atoms (P/N)) is estimated between ∼0.08–0.10 in PPy1 to PPy4.

For device studies, a silver contact on PPy served as the top contact while platinum is used as the bottom contact. Impedance measurements were performed using an Agilent 4294A precision impedance analyser in the range of 40 Hz–50 MHz. Room temperature micro-Raman studies on these samples were carried out in back-scattering geometry using a Horiba Jobin Yvon LabRAM HR instrument equipped with a charge coupled device detector (CCD) at a working temperature of −70 °C. The samples were illuminated by 514.5 nm line of an argon ion laser focused using a 100× objective on the samples. Experimental data was recorded using less than 3 mW of laser power (at the laser head) and for 10 s acquisition (per window) time. The spectral resolution was 0.4 $cm^{-1}$. Care was taken by using low intensities to avoid the sample burning. Raman spectra thus obtained is refined using Origin 9.0 mentioned in the following section.

## 3. Results and discussions

The variation in ac conductivity with disorder has been reported in different amorphous systems in a previous study [18]. The frequency dependence of conductivity for different PPy samples at zero applied bias is shown in figure 1(*a*); the inset of figure 1(*b*) shows the device structure through which measurements are done. The data is normalized with dc conductivity, $\sigma(0)$ to observe the relative response. The frequency dependency of the conductivity follows a power law: $\sigma(\omega) = A\omega^s$, where $A$ is a temperature-dependent constant and $s$ is both the frequency- and temperature-dependent exponent. Generally a threshold frequency, called onset frequency, $\omega_o$ is specified to the system below which conductivity remains nearly constant. It can be seen that the conductivity of all PPy samples is almost constant up to their respective onset frequency, and starts shooting up at higher frequencies which is a typically observed disorder system [18, 26]. The onset frequency is a useful parameter for probing the disorder in terms of nanoscale connectivity in the polymer films [27, 28]. A correlation length is defined as the length scale between the junctions through which charge transport takes place in disordered systems. Higher onset frequency is an indication of smaller correlation lengths, which gives rise to better connectivity and less disorder in the system. From the figure 1(*a*), the roughly estimated value of $\omega_o$ for PPy1 is $>10^7$ Hz, $\omega_o \sim 10^7$ Hz for PPy2 and PPy3, and $\omega_o \sim 10^6$ Hz for PPy4. This suggests that disorder varies in PPy films and decreases with higher synthesis temperature in normal-to-plane direction, as observed recently in electrochemically synthesized PPy [19]. The inset of figure 1(*a*) shows the frequency dependence of real part of $Z$, [Re($Z$)]. It can be seen that Re($Z$) for the PPy1, PPy2 and PPy3 is almost constant below their respective onset frequencies, but in the case of PPy4, Re($Z$) is nearly constant up to ∼10 kHz and increases gradually below this value. Figure 1(*b*) shows the frequency

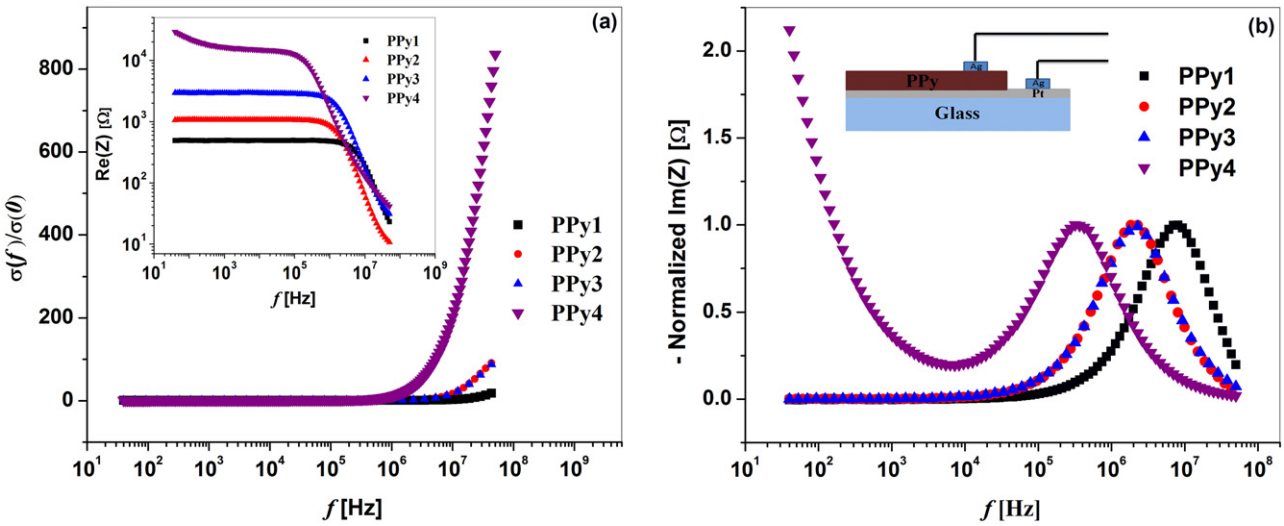


**Figure 1.** (*a*) Frequency dependence of normalized conductance, and inset shows the variation in resistance, Re($Z$) with frequency for different PPy samples. (*b*) Frequency dependence of rescaled reactance and inset shows the device structure.

dependence of normalized reactance [Im($Z$)] for different PPy samples. The existence of a single relaxation mechanism is observed in PPy1, PPy2 and PPy3, while two relaxation peaks are seen in the case of PPy4. The appearance of one or more relaxation peaks in the reactance plot is indicative of one or more relaxation processes, which suggest the formation of different phases such as grains and grain granular boundaries [15, 28]. The relaxation frequency is found to be decreasing from PPy1 to PPy4, which indicates that relaxation time of the charge carriers varies with disorder.

Impedance spectroscopy is a well-developed and widely accepted technique, which can describe a solid state device through an equivalent circuit to understand transport phenomena under various conditions. Impedance measurements in Cole–Cole representation of PPy1 at different voltages with platinum (Pt) being positively biased are shown in figure 2(*a*). The frequency is an implicit variable in this measurement and varied from 40 Hz to 50 MHz. Usually the data resemble the shape of an arc of a circle with the centre on or below the axis of Re($Z$). The data can be modelled with one simple parallel $RC$ circuit with a resistor ($R_\mathrm{p}$) and a capacitor ($C_\mathrm{p}$) connected in parallel as shown in figure 2(*a*). The $R_\mathrm{p}$ is associated with the material layer resistance and $C_\mathrm{p}$ is related to geometric capacitance of the layer (PPy in this case). However, due to the mismatch between the Fermi level of the contact electrode and polymer material, a contact resistance is usually present in all practical devices. Therefore, a series resistance ($R_\mathrm{s}$) is considered in addition to $R_\mathrm{p}$ and $C_\mathrm{p}$, when the data is simulated. In the presence of $R_\mathrm{s}$ the impedance of the circuit can be given by

$$Z = \left(R_\mathrm{s} + \frac{R_\mathrm{p}}{1+\omega^2 R_\mathrm{p}^2 C_\mathrm{p}^2}\right) - \mathrm{j}\left(\frac{\omega R_\mathrm{p}^2 C_\mathrm{p}}{1+\omega^2 R_\mathrm{p}^2 C_\mathrm{p}^2}\right) = Z' + \mathrm{i}Z''. \tag{1}$$

The impedance data for PPy1 is simulated with this circuit and is shown in figure 2(*a*). The values of different components ($R_\mathrm{s}$, $R_\mathrm{p}$, $C_\mathrm{p}$) used for simulating curves under different bias are presented in table 1. In the simulation, $R_\mathrm{s}$ decides the position, $R_\mathrm{p}$ decides the size and $C_\mathrm{p}$ decides the completeness of the semicircle. Since more carriers are injected into the layer with more bias, $R_\mathrm{p}$ decreases significantly when dc bias is raised, while $C_\mathrm{p}$ of the layer remains rather constant. This indicates the presence of space charge limited current in the device. It can be seen that the curves from the impedance data are not perfect semicircles and this simulation does not follow the measurements exactly. Similar deviations in fittings of impedance data using the equivalent circuit of figure 2(*a*) have been observed previously in the conductively doped carrier-transport layer [29, 30]. It is remarked that the imperfect fittings might result from the frequency dependence of the dielectric properties and spatial inhomogeneities in the thickness and dopant concentration, whose effects are not considered by a simple equivalent circuit of figure 2(*a*). According to MacDonald *et al*, this spatial inhomogeneity along with local processes such as diffusion leads to the origin of distributed relaxation time of the carriers, which causes a skewed or suppressed semicircle in Cole–Cole plot [31]. This distribution of time scales is difficult to model with simple parallel $RC$ circuit, so to account for the deviation in Cole–Cole plot, a CPE is introduced in place of the capacitor [29, 31]. CPE takes account of the dispersive properties such as frequency-dependent dielectric properties and provides the better modelling for the impedance characteristics of disordered materials. CPE has the impedance in the form of $Z_Q = (\mathrm{j}\omega)^{-\phi}/Q$, where $Q$ is a constant and $\phi$ is the exponent with a value between $0 < \phi < 1$. The exponent $\phi$ describes the degree of capacitive nature of the component. Now the total impedance of the $RQ$ circuit without a series resistance can be written as [32]

$$Z_\mathrm{CPE} = \frac{R_\mathrm{p}}{1+(\mathrm{j}\omega)^{\phi} Q_\mathrm{p} R_\mathrm{p}}. \tag{2}$$

Figure 2(*b*) shows the modified parallel $RQ$ equivalent circuit with a series resistance $R_\mathrm{s}$ and the simulated data for the PPy1. Fitting to the measured impedance data is improved significantly in comparison to the simple parallel $RC$ circuit.

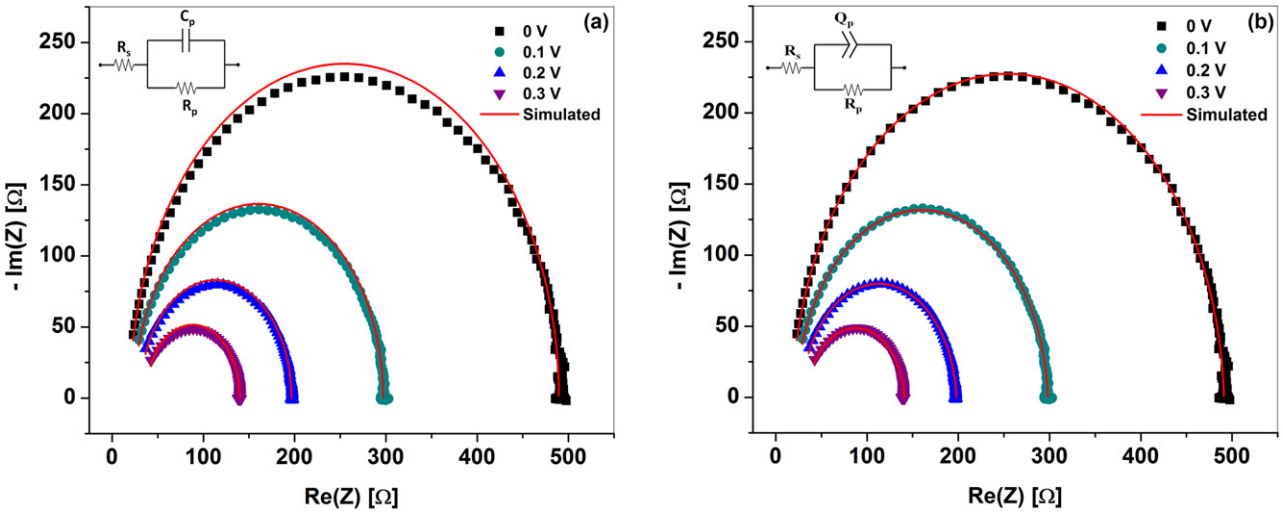


**Figure 2.** (*a*) Optimized fitting to the measured Cole–Cole plots at different bias for PPy1 using equivalent circuit consisting of *RC* element as shown in the inset. (*b*) Optimized fitting using equivalent circuit consisting of *RQ* element as shown in the inset.

**Table 1.** Parameters used to simulate measured Cole–Cole plot of PPy1 using *RC* circuit.

| Bias (V) | $R_s$ (Ω) | $C_p$ (F) | $R_p$ (Ω) |
|---|---|---|---|
| 0 | 19.5 | $1.0 \times 10^{-8}$ | 470 |
| 0.1 | 24 | $1.0 \times 10^{-8}$ | 273 |
| 0.2 | 30.5 | $1.0 \times 10^{-8}$ | 166 |
| 0.3 | 37 | $1.0 \times 10^{-8}$ | 103 |

**Table 2.** Parameters used to simulate measured Cole–Cole plot of PPy1 using *RQ* circuit.

| Bias (V) | $R_s$ (Ω) | $\phi$ | $Q_p$ (F $s^{\phi-1}$) | $R_p$ (Ω) |
|---|---|---|---|---|
| 0 | 18 | 0.975 | $1.0 \times 10^{-8}$ | 473 |
| 0.1 | 22 | 0.970 | $1.0 \times 10^{-8}$ | 276 |
| 0.2 | 28 | 0.96 | $1.0 \times 10^{-8}$ | 170 |
| 0.3 | 34 | 0.94 | $1.0 \times 10^{-8}$ | 107 |

The values of all the components and parameters used for the simulation are presented in table 2. The exponent $\phi$ varies from 0.94 to 0.975 with decrease in applied bias. Similarly, one skewed semicircle is observed in impedance measurements of PPy2 and PPy3 at different voltage bias and found to fit better with the simulation carried out through parallel *RQ* circuit with increased values of $R_p$, and decreased value of $Q_p$ and $\phi$. Since a skewed semicircle reflects the spatial inhomogeneity, $\phi$ can give a measure of disorder originating due to these inhomogeneities, and a low value of $\phi$ shows more disorder in the device [33].

Figure 3 shows the measured Cole–Cole plots of PPy4 device under different applied voltage bias. In contrast to other PPy devices synthesized at higher temperatures, PPy4 exhibits one semicircle and an arc of circle. Both are found to shrink at different rates with increase in dc bias. The semicircle (towards higher frequencies) is due to the impedance of the polymer layer and the arc towards lower frequencies can be related to polymer/electrode interfaces. A Cole–Cole plot with two semicircles can be modelled with an equivalent circuit consisting of a series connection between two parallel *RC* circuits (as shown in figure 3(*a*)). This is usually associated with a device comprising two separate structural regions with different electrical characteristics. It has been previously reported that a depletion region could occur near to the electrode with larger energy level mismatch in the doped conducting organic layer [29]. In such cases, $R1$ and $C1$ describe the resistance and capacitance of the depletion layer at the interface, while $R2$ and $C2$ represent the resistance and capacitance of the conducting bulk material. The simulated fittings to the measured impedance data using such an equivalent circuit under different dc biases is shown in figure 3(*a*) and the fitting parameters are listed in table 3. It is seen that again a satisfactory fitting to the data is difficult to obtain for a wide range of dc bias and frequencies with two *RC* circuits in the series. The simulated curves do not comply with the measured data suggesting that the equivalent circuit considered is not complete enough to model the impedance measurements of PPy4. Therefore, due to the lack in accuracy, the obtained parameters cannot be relied on to manifest the real situation in the device. This shows that simple parallel *RC* circuits do not include the effect of frequency dependence of electrical properties and spatial inhomogeneity in the device as also observed in case of PPy1. To account for a similar situation in the case of PPy4, $C1$ and $C2$ are replaced with two CPEs, $Q1$ and $Q2$ and a rather good fitting is obtained. Figure 3(*b*) shows the optimized fitting to the measured impedance data for the PPy4 under different bias and the equivalent circuit used for the simulation. The values of the circuit components and other parameters used for the simulation are presented in table 4.

The variation of the imaginary part of the impedance as a function of frequency under different dc bias is shown in figure 4, for PPy1 and PPy4. In the case of PPy1, only one peak is observed, which shifts towards higher frequencies and the magnitude of the peak shrinks with increase in dc bias (see figure 4(*a*)). Similar behaviour is observed for PPy2 and PPy3. But in the case of PPy4, two peaks appear in reactance spectrum as shown in figure 4(*b*). The first peak

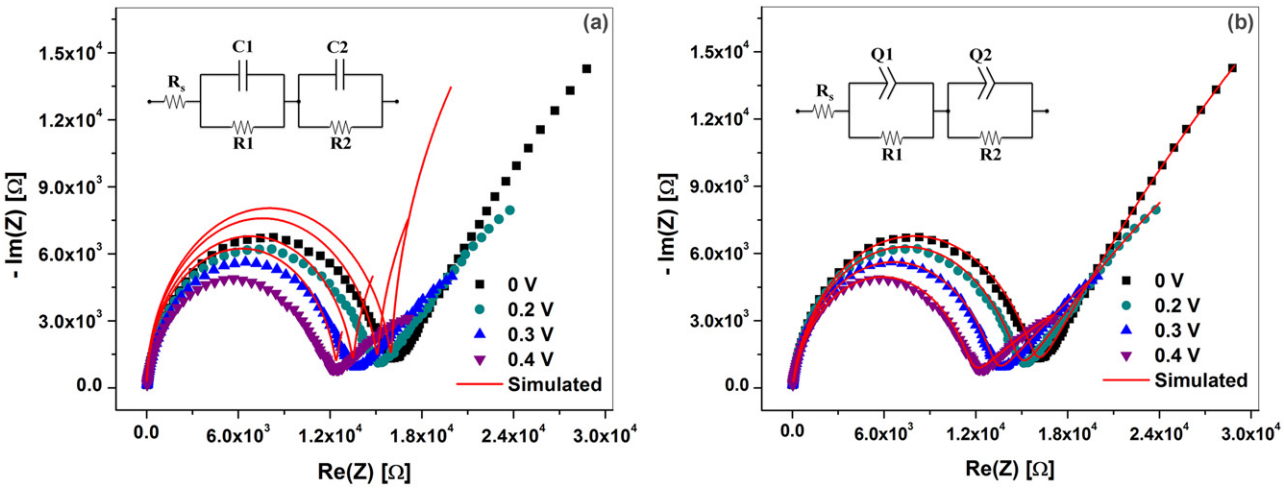


**Figure 3.** (*a*) Optimized fitting to the measured Cole–Cole plots at different bias for PPy4 using equivalent circuit consisting of two *RC* elements as shown in the inset. (*b*) Optimized fitting using equivalent circuit consisting of two *RQ* element as shown in inset.

**Table 3.** Parameters used to simulate measured Cole–Cole plot for PPy4 using two *RC* circuits.

| Bias (V) | $R_s$ (Ω) | $C1$ (F) | $R1$ (kΩ) | $C2$ (F) | $R2$ (kΩ) |
|---|---|---|---|---|---|
| 0 | 20 | $4.0 \times 10^{-9}$ | 50 | $1.0 \times 10^{-11}$ | 16.0 |
| 0.2 | 20 | $4.0 \times 10^{-9}$ | 30 | $1.0 \times 10^{-11}$ | 15.1 |
| 0.3 | 20 | $4.0 \times 10^{-9}$ | 20 | $1.0 \times 10^{-11}$ | 13.5 |
| 0.4 | 20 | $4.0 \times 10^{-9}$ | 15 | $1.0 \times 10^{-11}$ | 12.4 |

starts to appear at lower frequencies but the complete peak is not visible in the measured frequency range, while the second peak appears towards the higher frequency region as observed in other PPy devices. The peak observed at higher frequency corresponds to relaxation process in bulk layer while the peak appearing at lower frequency gives insight about relaxation at the metal/polymer interface [34]. This tells us that the carrier's relaxation time at the interface is much higher than in bulk. With increase in dc bias, both the peaks shift to higher frequency, while the magnitude of the peak that corresponds to interfacial states decreases faster than the magnitude of the peak corresponding to bulk. The value of the relaxation frequency ($f_r$) is deduced from peak position in the reactance spectrum and the relaxation time, $\tau_p$ is calculated using the relation, $\tau_p = 1/(2\pi f_r)$. The values obtained for $\tau_p$ are found to be ∼0.02 $\mu$s for PPy1, ∼0.08 $\mu$s for PPy2 and PPy3 and ∼0.46 $\mu$s for PPy4. Since the capacitance value of the bulk layer from the simulated equivalents circuits of all PPy devices is found to be almost constant with bias, space charge limited conduction is expected in these samples [35]. In space charge limited conduction, $\tau_p$ can be useful in an approximate estimation of mobility, $\mu$ given by the relation [34, 36]

$$\mu = \frac{L^2}{\tau_p V} \tag{3}$$

where $L$ is thickness of the device and $V$ is the applied bias. Mobility obtained with this technique is found to vary from 5 to 0.2 $cm^2\ V^{-1}\ s^{-1}$ in PPy1 to PPy4 at 0.1 V. With increasing bias, mobility increases in PPy samples since peak shifts toward higher frequency and relaxation time decrease. These mobility values infer that even if doping concentration is nearly the same in the polymer devices, disorder plays a crucial role in deciding the transport properties.

Figure 5 shows the micro-Raman spectra of all PPy films on platinum substrate. The spectra are smoothed using Savitzky–Golay method with 100 point window and fourth-order polynomial. The spectra are scaled by taking maximum intensity peak around 1600 $cm^{-1}$ to be equal to 100. These spectra are then de-convoluted using Gaussian line shape to obtain best fit parameter (reduced chi squared) between 0.4 and 1.3. The parameters extracted from the fitting are peak shift, full-width at half-maximum (FWHM) and peak height. A high signal-to-noise ratio over a weak 'fluorescence' background is observed. The high intensity peak at ∼1600 $cm^{-1}$ is ascribed to symmetric stretching of aromatic C=C ring. It can be seen from the figure that the peak shifts towards higher frequency side in PPy4, which suggests that PPy4 has more oxidized species compared to other samples. Since syntheses of these polymers were via anodic oxidative electropolymerization, relatively high oxidation is expected in the samples. A pronounced shoulder formation at higher wave number side of the 1600 $cm^{-1}$ band in PPy3 and PPy4 suggests that there may be some neutral species [24, 25, 37]. Similar observations have been made by Jenden *et al* on p-toluene sulfonate-doped PPy films [24]. This could be possible because at lower synthesis temperatures, migration and conformation of $PF_6^-$ ions may vary in polymer films. C=C band is important while studying conjugation length and oxidation state [38, 39]; therefore, these bands are de-convoluted as shown in figure 6. The other interesting observation from figure 5 is that the band at ∼1240 $cm^{-1}$ which is prominent and well-resolved in the case of PPy1, shifts towards the high frequency side and merges with other peaks at ∼1330 $cm^{-1}$ in PPy4. Similar kinds of observations have been reported in PPy under different conditions, but the explicit assignment of this band is not studied [37, 38, 40]. In some other studies, this band is assigned to the C=C stretching of PPy and platinum–olefin complex [41, 42], but PPy is environmentally stable

**Table 4.** Parameters used to simulate measured Cole–Cole plot for PPy4 using two *RQ* circuits.

| Bias (V) | $R_s$ (Ω) | $\phi 1$ | $Q1$ (F $s^{\phi 1-1}$) | $R1$ (kΩ) | $\phi 2$ | $Q2$ (F $s^{\phi 2-1}$) | $R2$ (kΩ) |
|---|---|---|---|---|---|---|---|
| 0 | 20 | 0.59 | $1.05 \times 10^{-6}$ | 155 | 0.90 | $8.0 \times 10^{-11}$ | 15.65 |
| 0.2 | 20 | 0.52 | $2.50 \times 10^{-6}$ | 90 | 0.90 | $8.0 \times 10^{-11}$ | 14.50 |
| 0.3 | 20 | 0.45 | $6.00 \times 10^{-6}$ | 70 | 0.90 | $8.0 \times 10^{-11}$ | 12.90 |
| 0.4 | 20 | 0.40 | $9.50 \times 10^{-6}$ | 35 | 0.90 | $8.0 \times 10^{-11}$ | 11.30 |

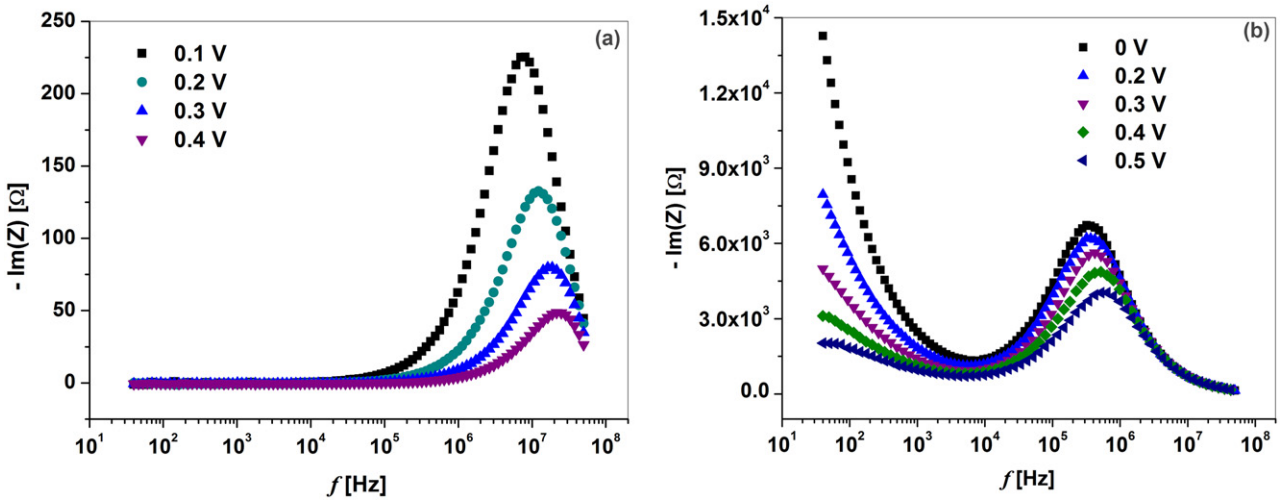


**Figure 4.** Reactance, Im($Z$) as a function of frequency at different bias ($a$) for PPy1, ($b$) for PPy4.

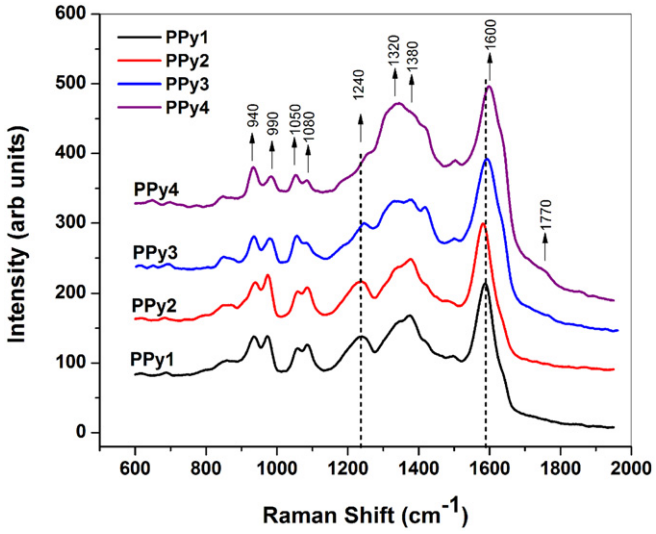


**Figure 5.** Raman spectra obtained for PPy films grown at different temperatures.

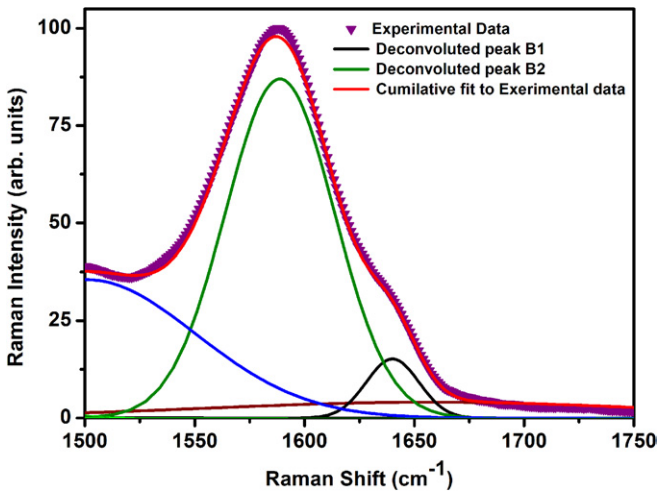


**Figure 6.** De-convoluted Raman spectra of PPy4 showing B1 and B2 bands.

so the possibility of complex formation with platinum is not considered in our case. The double peaks at ∼1050 and 1080 $cm^{-1}$ are assigned to C–H in-plane deformation. The other double peaks at ∼1320 and 1380 $cm^{-1}$ are attributed to the ring-stretching mode of PPy. Out of these assigned peaks, 1080 and 1380 $cm^{-1}$ peaks are because of the oxidized PPy. The bands ∼940 $cm^{-1}$ and 990 $cm^{-1}$ are assigned to the ring deformation associated with di-cations (bipolaron) and radical cations (polarons), respectively [37]. The intensities of these peaks give information about the presence of the respective species. We observe that their intensity ratio differs in PPy with synthesis temperature.

Figure 6 shows Raman spectra of PPy4 depicting the de-convoluted part of the C=C band. High wave number side peak corresponds to neutral species of PPy denoted as B1 and low wave number peak, B2 corresponds to oxidized species. Table 5 gives a list of parameters extracted from the de-convoluted peaks with the errors involved. FWHM of the de-convoluted peaks is attributed to the change in distribution of the conjugation length in the PPy films. We see from table 5 that FWHM of B2 band is largest for PPy4, which suggests that this film has more variation in distribution of conjugation length [37, 43]. The distribution in conjugation length can be attributed to the inhomogeneity and disorder in polymers. The intensity ratio between neutral and oxidized species shows

**Table 5.** Parameters obtained from de-convoluted Raman spectra.

| Sample | Peak shift (B1) ($cm^{-1}$) ±0.4 | Peak Height | FWHM (B1) ($cm^{-1}$) ±0.4 | Peak shift (B2) ($cm^{-1}$) ±0.4 | Peak Height | FWHM (B2) ($cm^{-1}$) ±0.4 | Peak Height Ratio B1/B2 |
|---|---|---|---|---|---|---|---|
| PPy1 | 1640.1 | 15.2 | 28.3 | 1588.8 | 86.9 | 58.4 | 0.17 |
| PPy2 | 1634.6 | 16.3 | 36.3 | 1583.5 | 82.8 | 56.2 | 0.20 |
| PPy3 | 1640.9 | 12.4 | 23.9 | 1594.8 | 90.3 | 76.7 | 0.14 |
| PPy4 | 1622.9 | 44.5 | 71.7 | 1589.5 | 58.6 | 78.8 | 0.76 |

that PPy1, PPy2 and PPy3 have nearly the same ratio, while this value is relatively high for PPy4. Since the presence of more oxidized species aids more conductivity, PPy1, PPy2 and PPy3 are expected to be more conductive than PPy4, which is reflected in the transport measurements. Raman peak shift can be attributed to different origins. Both morphological and conformational aspects contribute to Raman peak shift in polymers. A complicated morphology introduces more and more strain on the C=C bond and the peak shifts towards larger wave number side, hence peak shift can be attributed to disorder.

From the above discussions, it can be inferred that PPy4 has more disorder in comparison with other PPy films in out-of-plane geometry. It is well known that disorder decreases with lower synthesis temperature in free-standing PPy films in in-plane geometry [3, 4]. But in the present study, disorder is found to increase with synthesis temperature in out-of-plane geometry, which indicates the presence of anisotropy in the electropolymerized polymer films. This is supported by impedance measurements reported in this communication as well as low-temperature conductivity measurements from our previous report [19]. Similar observations of anisotropy in p-toluene sulfonate-doped PPy free-standing films has been made in early research on CPs, where conductivity and x-ray diffraction study are well correlated through disorder along and across geometry of the plane [44]. But in the present report, impedance and Raman studies are successfully adopted to characterize the interface and bulk properties through the thickness direction of the PPy devices, which is well correlated to disorder probed by the two techniques. A study of such anisotropic phenomena in CPs is quite interesting and important for developing the materials for applicative device purposes.

## 4. Conclusions

In summary, an effort is made to correlate the transport properties by probing disorder via two different spectroscopic techniques, impedance and Raman. Frequency dependence of both real and imaginary part has shown that disorder and inhomogeneity varies in different PPy devices, which thus affect the transport properties such as conductivity and mobility. Both impedance and Raman spectroscopies have deduced that in out-of-plane geometry, conductivity decreases in PPy devices as the synthesis temperature decreases. Mobility values along the thickness direction for each sample reveal the impact of disorder on out-of-plane geometry. A circuit containing CPE element is successfully used to obtain the best fit for the Cole–Cole plot of various PPy devices. The formation of a depletion layer is observed in PPy4, which can be correlated to the inhomogeneity occurring due to variation in distribution of conjugation length of the PPy chains and conformation of$PF_6^-$ in the polymer film.

## References


[1] Taylor P, Movaghar B, Pohlmann B and Schirmacher W 1980 *Phil. Mag.* B **41** 49
[2] Jaiswal M and Menon R 2006 *Polym. Int.* **55** 1371
[3] Yoon C O, Sung H K, Kim J H, Barsoukov E, Kim J H and Lee H 1999 *Synth. Met.* **99** 201
[4] Yoon C O, Reghu M and Moses D H A J 1994 *Phys. Rev.* B **49** 851
[5] Malinauskas A 2006 *Electrochim. Acta* **51** 6025
[6] Smela E 1999 *J. Micromech. Microeng.* **9** 1
[7] Bose S, Kim N H, Kuila T, Lau K and Lee J H 2011 *Nanotechnology* **22** 295202
[8] Punero S, Paserini S and Scrosuti B 1990 *Adv. Mater.* **2** 480
[9] Cervini R, Cheng Y and Simon G 2004 *J. Phys. D: Appl. Phys.* **37** 13
[10] Bufon C C B and Heinzel T 2006 *Appl. Phys. Lett.* **89** 012104
[11] Cesar C, Bufon B, Vollmer J, Heinzel T, Espindola P and John H 2005 *J. Phys. Chem.* B **109** 19191
[12] Qi G, Huang L and Wang H 2012 *Chem. Commun.* **48** 8246
[13] Anjaneyulu P, Sangeeth C S S and Menon R 2011 *J. Appl. Phys.* **107** 093716
[14] Garcia-Belmonte G, Munar A, Barea E M, Bisquert J, Ugarte I and Pacios R 2008 *Org. Electron.* **9** 847
[15] Idrees M, Nadeem M, Mehmood M, Atif M, Chae K H and Hassan M M 2011 *J. Phys. D: Appl. Phys.* **44** 105401
[16] Huang W, Peng J, Wang L, Wang J and Cao Y 2008 *Appl. Phys. Lett.* **92** 013308
[17] Amemiya T, Hshimoto K and Fujishuma A 1994 *J. Electroanal. Chem.* **377** 143
[18] Sangeeth C S S, Jaiswal M and Menon R 2009 *J. Appl. Phys.* **105** 063713
[19] Varade V, Anjaneyulu P, Sangeeth C S S, Ramesh K P and Menon R 2013 *J. Appl. Phys.* **113** 023708
[20] Ferrari A C 2007 Raman spectroscopy of graphene and graphite *Solid State Commun.* **143** 47
[21] Carach C, Riisness I and Gordon M J 2012 *Appl. Phys. Lett.* **101** 083302
[22] Martín-Carrón L, de Andrés A, Martínez-Lope M J, Casais M T and Alonso J A 2002 *Phys. Rev.* B **66** 174303
[23] Honnavar G V, Prabhava S N and Ramesh K P 2013 *J. Non-Cryst. Solids* **370** 6
[24] Jenden C M, Davidson R G and Turner T G 1993 *Polymer* **34** 1649
[25] Zhong C J, Tian Z Q and Tian Z W 1990 *J. Phys. Chem.* **94** 2171
[26] Sangeeth C S S, Kannan R, Pillai V K and Menon R 2012 *J. Appl. Phys.* **112** 053706
[27] Kilbride B E, Coleman J N, Fraysse J, Fournet P and Cadek M 2002 *J. Appl. Phys.* **92** 4024

[28] Schmidt R, Eerenstein W, Winiecki T, Morrison F and Midgley P 2007 *Phys. Rev.* B **75** 245111
[29] Chen C-C, Huang B-C, Lin M-S, Lu Y-J, Cho T-Y, Chang C-H, Tien K-C, Liu S-H, Ke T-H and Wu C-C 2010 *Org. Electron.* **11** 1901
[30] Meier M, Karg S and Riess W 1997 *J. Appl. Phys.* **82** 1961
[31] Macdonald J R and Barsoukov E 2005 *Impedance Spectroscopy: Theory , Experiment, and Applications* (New York: Wiley)
[32] Leever B J, Bailey C, Marks T J, Hersam M C and Durstock M F 2012 *Adv. Energy Mater.* **2** 120
[33] Anjaneyulu P, Sangeeth C S S and Menon R 2011 *J. Phys. D: Appl. Phys.* **44** 315101
[34] Kim S H, Choi K, Lee H, Hwang D and Do L 2000 *J. Appl. Phys.* **87** 882
[35] Tripathi D C, Tripathi A K and Mohapatra Y N 2011 *Appl. Phys. Lett.* **98** 033304
[36] Mostany J and Scharifker B R 1997 *Synth. Met.* **87** 179
[37] Chen F, Shi G, Fu M, Qu L and Hong X 2003 *Synth. Met.* **132** 125
[38] Zhang J, Wang F and Shi G 2003 *J. Appl. Polym. Sci.* **89** 3390
[39] Bazzaoui E A, Aeiyach S, Aubard J and Marsault J P 1995 *J. Phys. Chem.* **99** 6628
[40] Mikat J, Orgzall I and Hochheimer H D 2002 *Phys. Rev.* B **65** 174202
[41] Lehr I L, Quinzani O V and Saidman S B 2009 *Mater. Chem. Phys.* **117** 250
[42] Powell D B, Scott J G V and Sheppard N 1972 *Spectrochim. Acta* A **28** 327
[43] Bukowska J and Jackowska K 1990 *Synth. Met.* **35** 143
[44] Cvetko B F, Brungs M P, Burford R P and Skyllas-Kazacos M 1987 *J. Appl. Electrochem.* **17** 1198



View publication stats